

# Experimental Evaluation of the Influence of Connection Typology on the Behavior of Steel Structures Under Fire

ALDINA SANTIAGO, LUIS SIMÕES DA SILVA, PAULO VILA REAL, GILBERTO VAZ  
and ANTÓNIO GAMERIO LOPES

The behavior of steel joints under fire loading is a subject that has only recently received special attention by the research community. In fact, as recently as 1995, the European pre-standard on the fire response of steel structures (CEN, 1995) deemed it unnecessary to assess the behavior of steel joints under fire conditions. This approach was supported by the argument that there is increased thermal mass at the joint area. However, observations from real fires show that, on several occasions, steel joints fail, particularly their tensile components (such as bolts or end plates), because of the high cooling strains induced by the distortional deformation of the connected members (Bailey, Lennon and Moore, 1999; Buchanan, 2002; Wald, Simões da Silva, Moore, Lennon, Chladna, Santiago, Benes, and Borges, 2006a).

The experimental results on the response of steel joints under fire conditions are relatively recent and limited, partly because of the high cost of fire tests and the limitations on the size of furnace used. The primary aim of these few fire tests was concentrated on obtaining the moment-rotation relationships of isolated joints and the test procedure followed the testing of isolated joints at room temperature (Lawson, 1990; Leston-Jones, 1997; Al-Jabri, 1999). Despite the importance of such tests, they do not reflect the behavior of a complete structure under an urban fire.

Unlike room temperature conditions, joint behavior cannot be adequately represented by a moment-rotation relationship alone. Many aspects of behavior occur due to the interaction between members, and system behavior cannot be predicted or observed in tests of isolated elements. Large variable axial forces combined with bending moment and shear force are induced in the connection as experimentally shown (Allam, Fahad, Liu, Burgess, Plank and Davies, 1999; Liu, Fahad and Davies, 2002). Furthermore, another aspect that should be considered in the study of real structures is the cooling phase of a natural fire and the inherent unloading effects on the structure. During this phase, the plastically deformed beam contracts significantly and some connection components experience tensile forces (Simões da Silva, Santiago, Vila Real and Moore, 2005).

Obtaining detailed experimental evidence of the behavior of steel members subjected to realistic fire conditions is quite difficult and expensive. Natural fire tests, such as the Cardington tests (Simões da Silva et al., 2005) are ideal as they reproduce reality very closely, but it is quite difficult to obtain detailed measurements of the mechanical response of individual members and to quantify the various parameters that control their behavior. To overcome the limitations of isolated member tests and avoid the complexity of fire tests on real structures, carrying out tests on steel subframes constitutes a good compromise. These allow the observation of the redistributions of forces that take place throughout the fire and, in a suitable installation, allow the reproduction of the transient temperature conditions that occur along the length of the members, including the proper consideration of the cooling phase.

The main objective of this paper is to describe an experimental test program carried out by the Department of Civil Engineering at the University of Coimbra on a steel subframe in order to evaluate the behavior of various types of steel joints under a natural fire and transient temperature conditions along the length of the beam. The tests were carried out on a purposely developed experimental installation that could reproduce the transient temperature conditions measured in the seventh Cardington test (Wald, Chladná, Moore, Santiago and Lennon, 2006b). The results of these tests provide invaluable evidence on how to design joints that are able to survive a fire.

---

Aldina Santiago is professor, department of civil engineering, University of Coimbra, Coimbra, Portugal.

Luis Simões Da Silva is professor, department of civil engineering, University of Coimbra, Coimbra, Portugal.

Paulo Vila Real is professor, department of civil engineering, University of Aveiro, Aveiro, Portugal.

Gilberto Vaz is professor, department of mechanical engineering, ISEC—Polytechnic Institute of Coimbra, Coimbra, Portugal.

António Gamerio Lopes is professor, department of mechanical engineering, University of Coimbra, Coimbra, Portugal.

---

## DESCRIPTION OF THE EXPERIMENTAL PROGRAM

### General Description

The experimental program consists of the testing of a series of subframes composed by two thermally insulated HEA300 (similar to W12×65) cross-section columns and an unprotected noncomposite IPE300 (similar to W12×26) cross-section beam with 5.70 m (18.7 ft) free span, supporting a concrete slab (Figure 1). These dimensions were chosen to reproduce the measured dimensions of a steel subframe from the fire compartment of the seventh Cardington fire test

(Wald et al., 2006a). The steel grade specified for the beam and columns is S355 and the beam cross-section is class 1 at room temperature as well as at elevated temperatures, i.e., compact shape, with adequate ductility for large plastic rotation and development of plastic moment (CEN, 2005a). The slab construction was of steel deck and light weight in-situ concrete composite floor and was intended to reproduce the thermal boundary condition in typical composite frames.

The steel subframe was supported by two reaction frames (Figure 1) perpendicular to the plane of the frame. They provided pinned supports at the top of the columns, allowing free axial movement; the bottom of the columns was hinged and fixed to a reinforced concrete footing that was secured

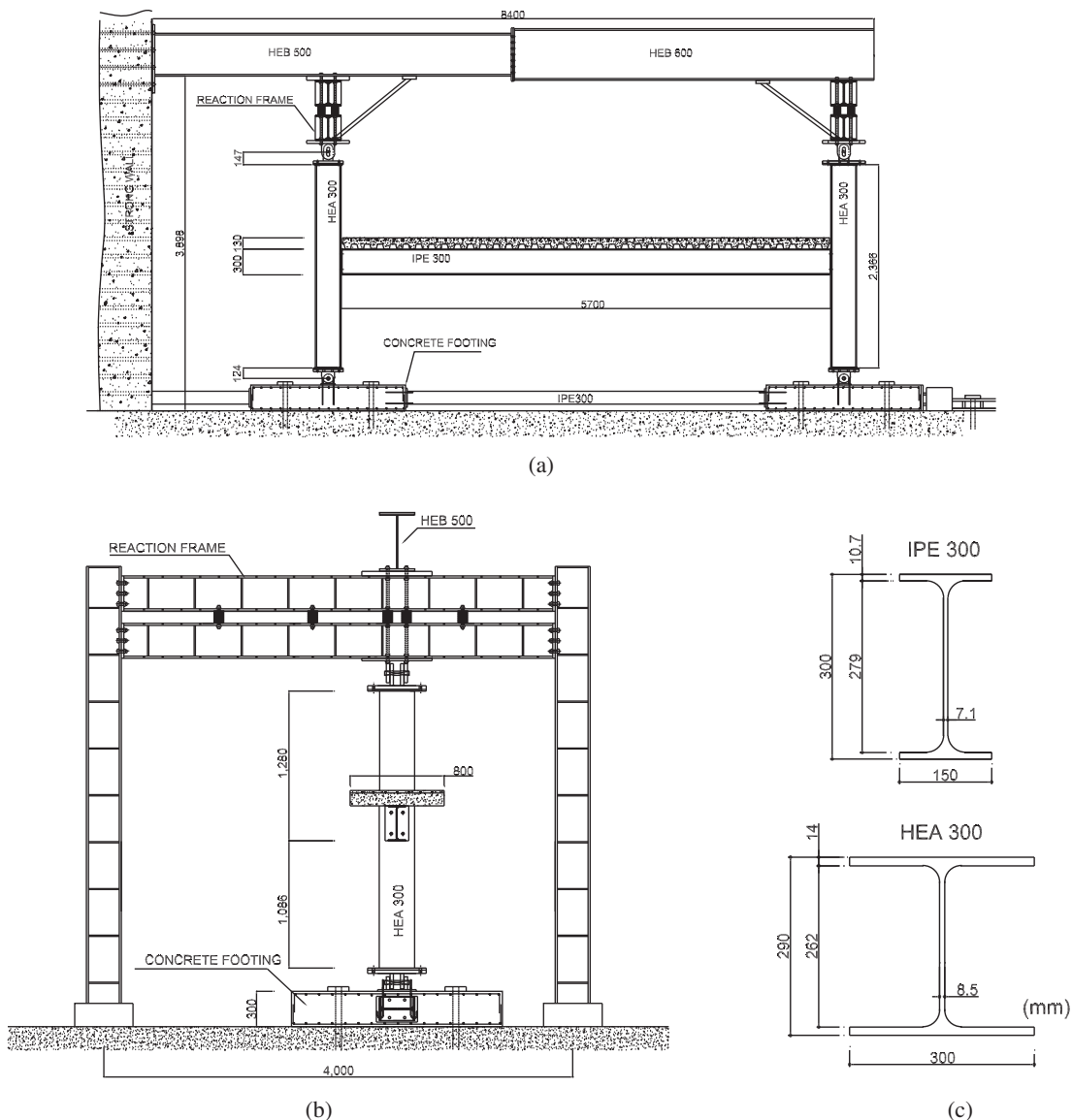


Fig. 1. General layout: (a) longitudinal view; (b) lateral view; (c) geometry of the profiles (1 in. = 25.4 mm).

Table 1. Test Program				
Test ID	Joint Typology	End plate Dimensions (mm) and Steel Grade	Bolts / Weld	Resistance
FJ01	Flush end plate	(320×200×10); S275	2 bolt row M20, 8.8	$M_{j,Rd} = 47.6$ kN-m (42.1 lbf-in.)
FJ02		(320×200×16); S275	2 bolt row M20, 10.9	$M_{j,Rd} = 93.0$ kN-m (82.3 lbf-in.)
FJ03		(320×200×16); S275	2 bolt row M20, 8.8	$M_{j,Rd} = 88.6$ kN-m (78.4 lbf-in.)
EJ01	Extended end plate	(385×200×16); S275	3 bolt row M20, 8.8	$M_{j,Rd} = 146.6$ kN-m (130 lbf-in.)
HJ01	Header plate	(260×150×8); S275	4 bolt row M20, 8.8	$V_{j,Rd} = 395.4$ kN (88,900 lbf)
WJ01	Welded joint	—	$a_f = a_w = 10$ mm (0.394 in.)	$M_{j,Rd} = 147.0$ kN-m (130 lbf-in.)

Note: Bolt class 8.8 ( $f_t = 92,824$  psi;  $f_u = 116,030$  psi); bolt class 10.9 ( $f_t = 130,533$  psi;  $f_u = 145,037$  psi); bolt size M20 (nominal size: 0.787 in); steel S275 (39,900 psi); steel S355 (51,500 psi).

in position by Dywidag bars passing through the laboratory strong floor and fixed horizontally using a steel profile connecting both reinforced concrete footings.

The two reaction frames were horizontally restrained at the top by connecting HEB 500 and HEB 600 profiles to the strong wall (Figure 1a). In order to avoid parasitic rotations at the top of the reaction frames and, consequently, mistakes in the measurements, bracing struts were positioned between the top of the reaction frames and the top beam acting as longitudinal bracing.

Lateral movement of the beam was prevented. The beam top flange was restrained at three points: at midspan, at

1500 mm (59.1 in.) to the left side from the midspan, and at 1500 mm to the right side from the midspan. The restraint system is illustrated in Figure 2 and vertical sliding movement is allowed.

### Experimental Program

The experimental program was comprised of six tests and the varied parameter was the beam-to-column connection configuration (Table 1). They were representative of usual joint typology used in building frames: header plate, flush and extended end plate; and welded (Figure 3). According to EN 1993-1-8, WJ01, FJ01, FJ02, FJ03 and EJ01 joints are

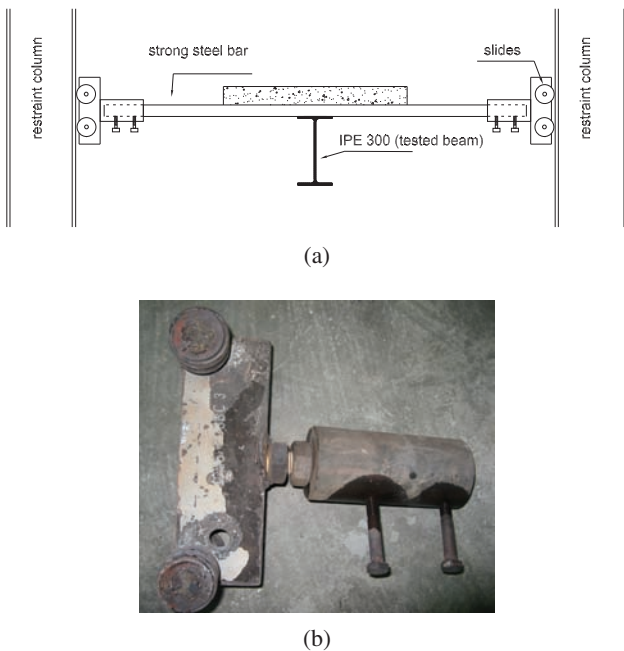


Fig. 2. (a) Lateral restraint system; (b) Detail of slide.

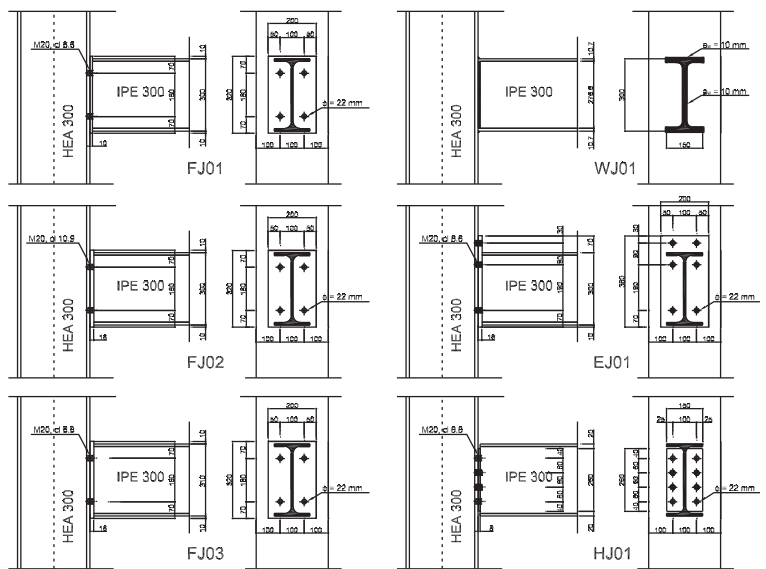


Fig. 3. Geometry of the joints (1 in. = 25.4 mm).

% maximum	C	Mn	Si	P	S	N	CEV
IPE 300	0.08	1.02	0.18	0.02	0.022	0.011	–
HEA 300	0.11	1.24	0.21	0.015	0.018	0.011	0.365

No. of tests	$\theta$ , °C	$E_{a,\theta}$ , GPa	$k_{E,\theta}$	$f_{p,\theta}$ , MPa	$k_{p,\theta}$	$f_{y,\theta}$ , MPa	$k_{y,\theta}$	$f_{u,\theta}$ , MPa	$k_{u,\theta}$	$\epsilon_{u,\theta}$ , %	$Z_{\theta}$ , %
4	20	210	1.00	382	0.99	388	1.01	494	1.00	30.8	63.2
2	100	192	0.91	412	1.06	374	0.96	490	0.99	24.9	66.9
2	200	189	0.90	347	0.90	439	1.15	571	1.15	15.5	52.5
3	300	177	0.84	283	0.73	392	1.03	570	1.15	21.8	48.8
3	400	168	0.80	254	0.66	361	0.95	478	0.97	18.4	52.1
3	500	124	0.59	218	0.56	318	0.83	371	0.75	19.2	39.3
2	600	105	0.50	176	0.45	215	0.56	222	0.45	16.0	27.5
2	700	39	0.19	85	0.22	118	0.31	147	0.30	27.4	73.4
3	800	18	0.09	41	0.11	48	0.13	51	0.10	37.1	37.2
2	900	2	0.01	23	0.06	48	0.12	37	0.07	23.7	18.8
3	1000	1	0.00	18	0.07	27	0.05	29	0.06	21.8	18.0

Note: 1 psi = 6895 MPa; °F = 1.8(°C) + 32

No. of tests	Bolts	$E$ , GPa		$f_y$ , MPa		$f_u$ , MPa		$\epsilon_u$ , %	
		$\mu$	COV %	$\mu$	COV %	$\mu$	COV %	$\mu$	COV %
6	8.8	211.2	2.8	657.7	7.7	834.2	1.8	1.42	25.6
3	10.9	211.6	1.0	860.0	0.2	1078.7	0.2	1.30	32.2

Note: 1 psi = 6895 MPa.

classified as partial strength and semi-rigid joints while the HJ01 joint is pinned (CEN, 2005b).

## Mechanical Properties

### Tensile Tests of the Steel Coupons

The test program included two different steel grades: S275 for the end plates (to match the Cardington Frame) and S355 for the steel sections. According to the European Standard EN 10025-1 (CEN, 2004), the steel qualities are S275JR and S355J2G3, respectively. Table 2 summarizes the chemical composition according to the supplied steel certificates.

The steady-state tests of the steel coupons extracted from the profiles were performed according to EN 10002-5 procedures (CEN, 1992). Each test specimen was heated up to a specific temperature and subsequently a tensile test was carried out. The relevant values are set out in Table 3. For each

temperature, Young's modulus,  $E_a$ , the yield and ultimate stresses,  $f_y$  and  $f_u$ , the ultimate strain,  $\epsilon_u$ , and the coefficient of area reduction,  $Z$ , are given. In addition, Table 3 includes the calculated values of the reduction factor for the slope of the linear elastic range  $k_{E,\theta} = E_{a,\theta}/E_a$ ; the reduction factor for effective yield strength  $k_{y,\theta} = f_{y,\theta}/f_y$ ; and the reduction factor for ultimate strength  $k_{u,\theta} = f_{u,\theta}/f_u$ . No coupon tests were carried out for the end plate material. Coupon tests showed that yield and ultimate stresses first decrease with increasing temperature and then increase at the temperature range of 200 to 300 °C (392 to 572 °F) before decreasing at higher temperature. Such behaviors are attributed to the dynamic strain aging (DSA), austenite to martensite transformation, and high-temperature softening in addition to the tempering of bainite. These results show a good comparison with EN 1993-1-2-2005 and with the results obtained by other authors, as described by Santiago (2008).

### Tensile Tests of the Bolts

Two different classes of M20 bolts were used in the experiments, 8.8 and 10.9. Several bolts from each group were tested in tension in order to determine the mechanical properties of the bolt material at room temperature. The average properties,  $\mu$ , and the corresponding coefficient of variation, COV, are set out in Table 4.

### Loading Definition

#### Mechanical Loading

The mechanical loading was applied at two points of the top flange of the noncomposite beam, 700 mm (27.6 in.) to either side of the beam midspan. Each concentrated load was equal to 20 kN (4,500 lbf), which corresponds to a live load ratio of 0.2. The load ratio is here defined as the ratio of the live load at fire limit state [ $M_{f,d} = 46 \text{ kN-m}$  (40.7 lbf-in.)] to the load-carrying capacity as a simply supported beam at room temperature [ $M_{Rd} = 223 \text{ kN-m}$  (197 lbf-in.)] based on a yield stress of 355 MPa (51,500 psi). This mechanical loading was applied using two pairs of concrete blocks at room temperature (Figure 4).

#### Thermal Loading

Thermal loading was applied to the beam and joints (from the beam side only). In order to prevent global structural instability, the columns were thermally protected by 1.18 in.

of ceramic fiber blanket [ $\lambda = 0.06 \text{ W/m-K}$  or  $0.035 \text{ Btu/(ft-h-}^\circ\text{F)}$ ] at  $\theta = 200 \text{ }^\circ\text{C}$  or  $392 \text{ }^\circ\text{F}$ ;  $\lambda = 0.27 \text{ W/m-K}$  or  $0.156 \text{ Btu/(ft-h-}^\circ\text{F)}$  at  $\theta = 1000 \text{ }^\circ\text{C}$  or  $1832 \text{ }^\circ\text{F}$ ], where  $\lambda$  denotes the coefficient of thermal conductivity for two different temperatures). Thermal loading was time dependent (heating and cooling phases) and was also variable along the beam span. The tested beams were divided into three heating zones: zone 1 (central zone), and zones 2 and 3 (end zones) (Figure 5). The beam temperature-time curves applied at each beam zone reproduced the values measured in a previous full-scale test (Wald et al., 2006a; Wald et al., 2006b) and they correspond to the measured temperatures at the beam bottom flange. Figure 5b illustrates the prescribed temperature-time curves for the three zones as well as the measured Cardington curve at midspan. The first 10 min of the full-scale fire were neglected because the corresponding temperatures were very low and difficult to reproduce (corresponding to ignition and prior to flashover). For safety reasons, the maximum temperature applied in the tests was  $900 \text{ }^\circ\text{C}$  ( $1652 \text{ }^\circ\text{F}$ ) at the beam bottom flange ( $35 \text{ min} < t < 50 \text{ min}$ ).

### Heating and Exhaust System

To apply the fire load, a special purpose heating system was developed—Natural Fire Facility (Santiago, Simões da Silva and Vila Real, 2008). This heating system consisted of 11 individual gas burners suspended along the beam span. The burners were fitted with externally controlled continuous



Fig. 4. General layout: (a) preparation; (b) during a fire test.

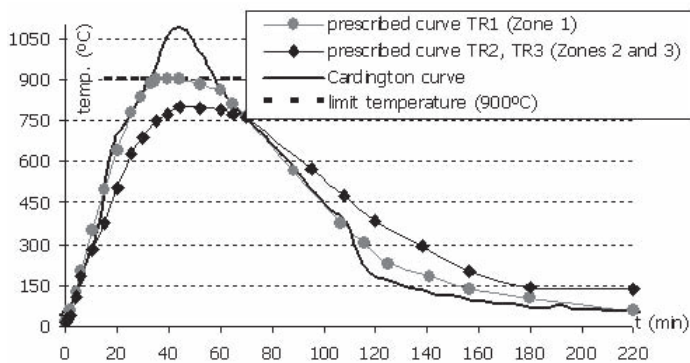
valves that controlled each zone individually and allowed specifying the range of the flame intensity, and thus reproduce the thermal load strategy (Figure 6). At the same time, control thermocouples at each zone were installed to measure instantaneously the temperature inside the steel. The gas delivered to the system was adjusted by comparing the thermal load strategy with the instantaneous temperature at each control thermocouple. The burners were fed by propane gas through flexible copper pipes (to allow adjustments at the support structure) and were supplied by a battery of gas reservoirs located outside the laboratory. Propane gas allows a definition of a yellow turbulent diffusion flame, common in urban fires. The main reasons this heating system was preferred to a furnace or an electric blanket were the possibility to achieve a direct heating by flame, allowing an easy control of the local thermal load; as the facility is open to the surroundings, a natural convection cooling flow is obtained and the overall setup is easier; and the temperature gradient along the beam is similar to what is observed in an urban fire, as already discussed.

In order to reduce the heat losses to the surroundings and the air entrainment to the vicinity of the beam, rock wool panels were fixed vertically from the exhaust system to the floor. The internal face of the rock wool was aluminized to reflect radiation (Figure 4). This way, the beam heated up not only because of direct incidence of flames but also through radiation from flames, and from the exhaust system and rock wool panels.

In order to allow the exhaust of smoke and combustion

Zone 2 TR2	Zone 1 TR1	Zone 3 TR3
1000	5680	1000

(a)



(b)

Fig. 5. Thermal loading: (a) definition of heating zones; (b) steel time-temperature curves of beam bottom flange.

gases, the system shown in Figure 4 was used. This exhaust system, fixed to the supporting structure, consists of a semi-circular steel shell around the top of the composite slab and closed at the ends. This semi-circular steel shell drove the combustion gases through flexible steel pipes to a ventilator that forced out these gases to the outside of the laboratory through an opening in the roof.



(a)



(b)



(c)

Fig. 6. (a) Individual gas burner; (b) heating system; (c) temperature control system.

## Instrumentation

The results were recorded by means of the following instrumentation: thermocouples, displacement transducers and thermographic cameras. Roughly 75 thermocouples of K type with two 0.5-mm (0.02-in.) wires were positioned inside the steel to monitor the temperature in the connected elements (end plate and bolts) and the temperature profiles across the beam and protected columns. The exact number of thermocouples depends on the joint geometry. In order to avoid the direct contact with the flames, the thermocouples attached to the heated beam and the connections were protected by ceramic rods (Figure 7).

Displacement transducers were used to measure displacements and deformations of the beam and columns. They measured beam deflection at mid-span and 300 mm (11.81 in.) away from the joints; horizontal movement of the columns external column flange at the level of the beam axis and the external column flange at the top and bottom ends; and residual displacements of the reaction frame. In the beam, measurements were made outside the fire zone using refractory glass, with a very low thermal expansion coefficient, and a sheaves system that bring the measurements out of the fire zone. A pair of 200-mm (7.87-in.) displacement transducers located at the mid-span of the beam was used to measure the maximum deflection (2×200 mm).

## Testing Procedure

The natural fire tests were transient tests. The testing procedure is characterized in two different and sequential steps. In step 1, the mechanical load was applied instantaneously and measurements were recorded. In step 2, the heating unit

was switched on. The mechanical loading was maintained constant and the thermal load was incremented according to the prescribed fire strategy.

## TESTS RESULTS

### Efficiency of the Natural Fire Facility

Figure 8 compares the prescribed fire curves (control system) with the temperatures measured at the beam reference points (TR1, TR2 and TR3) for test EJ01. Good agreement was observed. Similar results were observed for the other five tests.

### Temperature

#### Beam Temperature

Figure 9 depicts the temperature distribution across the beam mid-span cross section for test EJ01. Temperature measurements at mid-span of the beams were taken in the bottom flange (both sides), web and top flange. During the heating phase, the web and bottom flange temperatures are quite similar, despite the fact that the flames surround the bottom flange earlier, the reduced web thickness allowing a faster temperature increase. In the cooling phase, the web temperature decreases faster than the bottom flange temperature for the two following reasons: the reduced thickness corresponds to a lower thermal inertia; and during this phase, the length of flames reduces, and, from a certain moment in time onwards, they only surround the bottom flange. Because of the thermal inertia of the slab and its flame protection effect, the top flange showed the lowest temperature during the

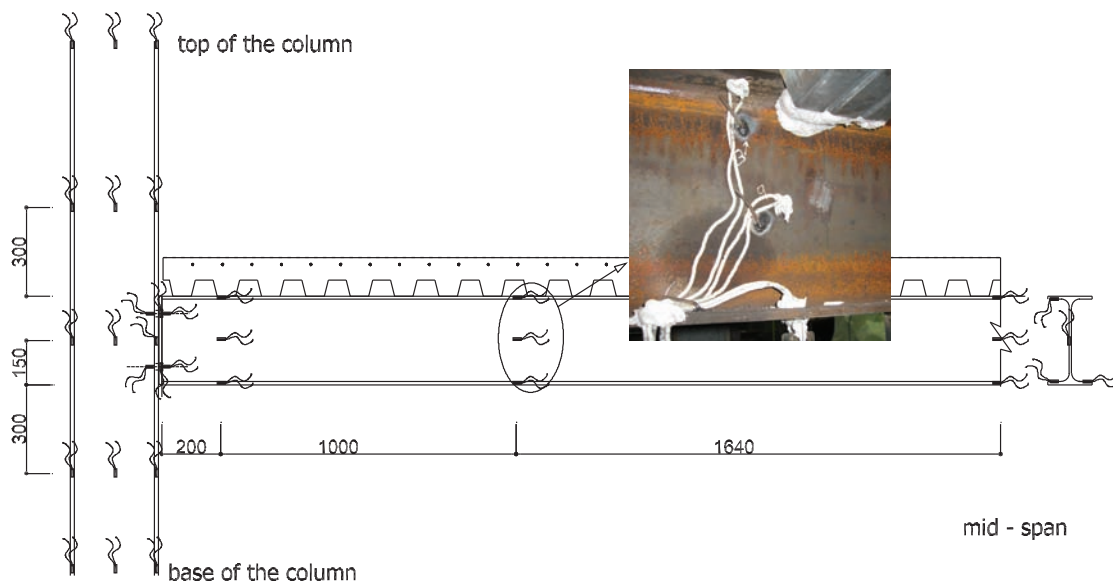


Fig. 7. Location of thermocouples and detail of thermocouples in the beam.

Table 5. Temperatures at Beam Mid-span									
Test Location		Temperature (°C)							
		15 min.	25 min.	40 min.	50 min.	60 min.	70 min.	80 min.	150 min.
FJ01	bottom flange	454	711	877	878	815	721	619	171
	web	346	694	878	873	801	669	538	144
	top flange	253	505	770	813	780	669	566	226
FJ02	bottom flange	493	730	896	886	867	753	647	183
	web	400	725	872	864	847	645	552	150
	top flange	(a)	(a)	(a)	(a)	(a)	(a)	(a)	(a)
FJ03	bottom flange	499	740	911	908	867	774	680	178
	web	423	730	871	852	792	680	568	162
	top flange	309	588	797	826	810	735	629	206
EJ01	bottom flange	452	727	890	898	845	710	605	152
	web	374	774	882	867	771	623	518	133
	top flange	231	555	763	785	769	677	571	178
HJ01	bottom flange	489	733	882	(b)	(b)	(b)	(b)	(b)
	web	394	718	845	(b)	(b)	(b)	(b)	(b)
	top flange	245	554	743	(b)	(b)	(b)	(b)	(b)
WJ01	bottom flange	478	732	904	914	888	784	679	166
	web	423	726	868	866	829	719	599	158
	top flange	326	613	787	813	815	733	614	208
Average	bottom flange	477	729	893	897	857	748	646	170
	web	393	728	869	864	808	667	555	149
	top flange	273	563	772	809	793	704	595	204
COV %	bottom flange	4.2	1.3	1.4	1.5	2.9	3.9	4.7	6.4
	web	7.5	3.5	1.5	0.8	3.3	4.9	4.9	7.1
	top flange	12	7.1	2.8	1.0	1.8	3.5	3.7	7.7

(a) not measured; (b) beam failure.

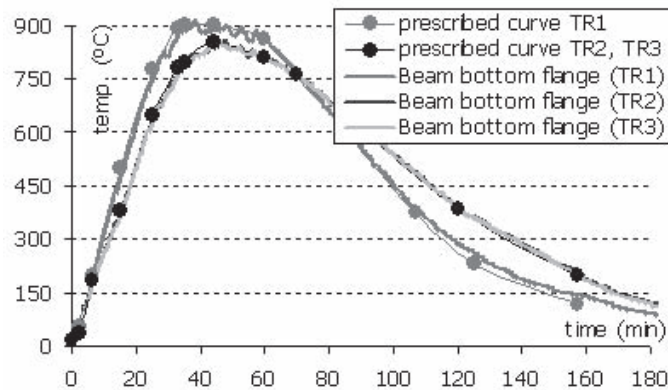


Fig. 8. Measured beam temperature versus prescribed fire curves (test FJ01).

heating phase with a maximum temperature of about 743 °C (1370 °F) and slower cooling, and the maximum top flange temperature was recorded during the cooling phase. Figure 10 was obtained using a thermographic camera. It illustrates the temperature distribution in the central zone of the beam during the heating phase. Table 5 summarizes the temperatures across the depth of the beams; for each test, three different cross-sections were measured: mid-span; at 1650 mm (65 in.) to the Z3 side from the mid-span; and at 1650 mm to the Z2 side from the mid-span. All tests showed similar temperature development during the fire. The average coefficient of variation, COV, is about 4.2%, while the maximum COV does not exceed 12%.

### Joint Temperature

Figure 11 compares the temperature-time variation across the depth of the beam 200 mm (7.9 in.) away from the connection Z3 with the bottom flange temperature at mid-span

(test EJ01). During the heating phase, the joint temperature was significantly lower than the mid-span bottom flange, which is usually the critical element that defines the limiting temperature of the beam. In contrast, the cooling down in the joint was slower, in accordance with what happens in a real fire situation (Wald et al., 2006b). The maximum temperature near the joints was measured in the bottom flange and corresponded to about 90% of the maximum temperature at mid-span.

Table 6 summarizes the temperatures across the depth of the beams 200 mm (7.9 in.) away from the face of the columns in zones Z2 and Z3. All tests show similar temperature development during the fire. The average coefficient of variation is about 3.6%, while the maximum coefficient of variation does not exceed 9.8%.

Figure 12 compares the temperature curves for the various connection elements of joints in zone Z3 (test EJ01). Measurements were made for each bolt row as follows: in the bolt (beam side); in the bolt shank under the nut (column

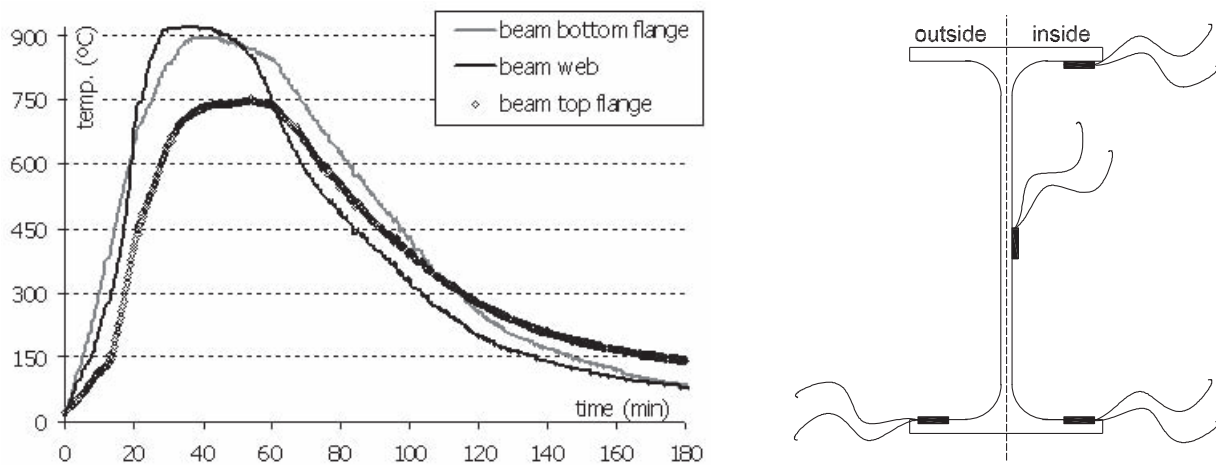


Fig. 9. Temperature distribution across the beam mid-span (test EJ01).

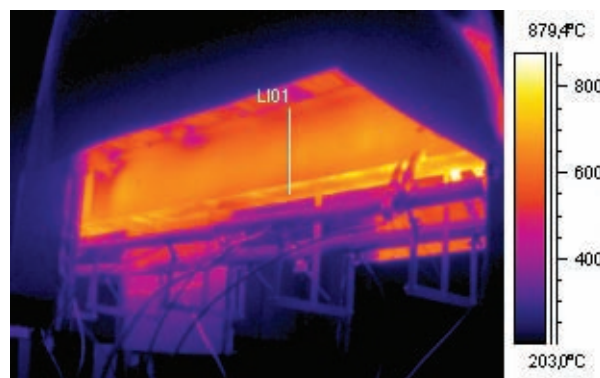


Fig. 10. Thermographic image of the temperature distribution in the beam during the heating phase.

Table 6. Temperatures at Beam Near the Connection (200 mm)									
Test Location		Temperature (°C)							
		15 min.	25 min.	40 min.	50 min.	60 min.	70 min.	80 min.	150 min.
FJ01	bottom flange	326	563	778	821	793	745	670	242
	web	290	587	788	790	735	635	540	206
	top flange	199	424	703	752	742	655	569	247
FJ02	bottom flange	359	612	751	784	783	748	677	234
	web	269	620	738	752	751	702	590	178
	top flange	195	453	666	672	687	687	607	256
FJ03	bottom flange	352	643	842	841	804	766	701	249
	web	298	599	783	782	731	670	589	215
	top flange	214	520	746	752	713	664	596	258
EJ01	bottom flange	379	660	841	847	813	761	686	236
	web	301	632	811	798	745	674	577	200
	top flange	202	555	763	764	720	670	593	241
HJ01	bottom flange	371	638	827	(b)	(b)	(b)	(b)	(b)
	web	269	560	737	(b)	(b)	(b)	(b)	(b)
	top flange	206	470	681	(b)	(b)	(b)	(b)	(b)
WJ01	bottom flange	363	615	822	836	798	753	684	236
	web	300	578	788	786	750	685	585	203
	top flange	191	472	731	750	715	674	592	246
Average	bottom flange	358	622	810	826	798	754	683	239
	web	288	596	774	781	742	673	576	200
	top flange	201	482	715	738	715	670	591	249
COV, %	bottom flange	5.2	6.0	5.1	2.6	1.1	1.2	1.6	2.2
	web	5.2	4.5	3.9	2.0	1.1	3.3	3.2	6.1
	top flange	4.1	9.8	5.3	4.5	2.4	1.6	2.1	2.6

(b) beam failure

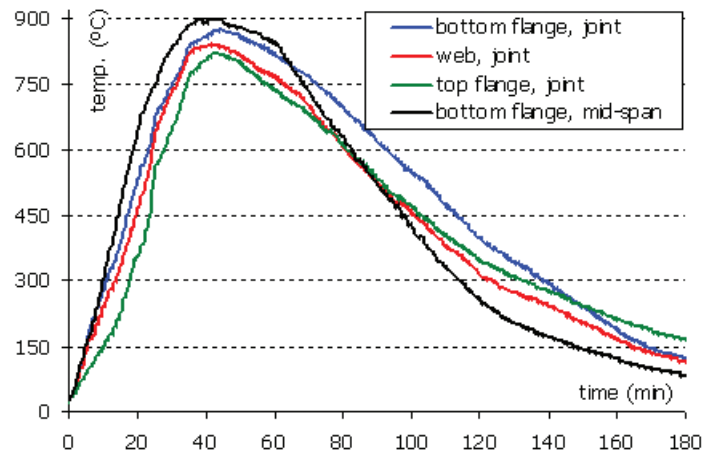


Fig. 11. Temperature in the beam near the joint Z3 (test EJ01).

side); and in the end plate at the same level of the bolt. Again, in the heating phase, the connection temperature was significantly lower than the remote bottom flange at mid-span; in contrast, the cooling down in the joint elements was slower, because of thermal inertia of the adjacent column and connection elements, and the different prescribed thermal loading applied at the joints section. The maximum temperature at the connection is thus reached during the cooling phase.

The first bolt row from the top was significantly cooler than the lower bolts, because the adjacent slab prevents the direct contact from the flames. Furthermore, the thermal inertia of the adjacent column acts as a heat sink. The end plate temperature was quite similar to that of the bolts head at the same level. Exception is made at the level of the second bolt row; in this case, the flames engaged the plate thermocouple more than the bolt head thermocouple and the end plate received more heat than the bolt head. This measurement should not be considered as representative of the average plate temperature at this level. Temperature gradient along the bolts was also measured: the maximum temperature in the head of the third bolt row was about 150 to 200 °C

(302 to 392 °F) higher than the corresponding shank; a maximum temperature of about 400 °C (752 °F) was measured in the shanks. For the first bolt row, a difference of about 60 °C (140 °F) on the maximum temperature is observed; this difference could be due to the temperature variation within the beam cross section. The effect of the heat transfer by conduction on the joint element is also evident: the bolt heads and plate heat up first, followed by the corresponding shanks.

### Structural Deformation

Figure 13 compares the evolution of the mid-span deflections during the fire. Most of the beams were able to sustain the load with reduced deflection up to 10 min [ $\theta_0 < 150$  °C (302 °F)]; during this stage, the deflection was mainly due to the mechanical loading. Beyond that, due to the loss of stiffness, the midspan deflection increased gradually. Beyond 20 min, a further rise in temperature [ $\theta_0 > 550$  °C (1022 °F)] led to a progressive run-away of the beam deflection as the loss of stiffness and strength accelerated. In the case of the FJ02, EJ01 and WJ01 tests, a maximum deflection of 375 mm (14.8 in.) was approximately reached (these values were measured already during the cooling phase). For the HJ01 test, Z3 joint collapsed during the heating phase of the fire [ $\theta_0 = 900$  °C (1652 °F)] as a result of the run-away deflection at high temperatures [ $\delta_{beam} = 393$  mm (15.5 in.)]. Once the cooling phase started, the heated beams began to recover strength and stiffness from an inelastic state, together with a reduction of thermal strains. This induced tensile, axial forces and the reversal of the deflection. Because of the limited range of the displacement transducers (400 mm), FJ01 curve was incomplete; however, a maximum deflection of 428 mm (16.9 in.) was measured at the end of the fire.

For the same reason, the maximum deflection at the mid-span of beam FJ03 was not measured, but during the cooling phase the deflection reduced to values lower than 400 mm

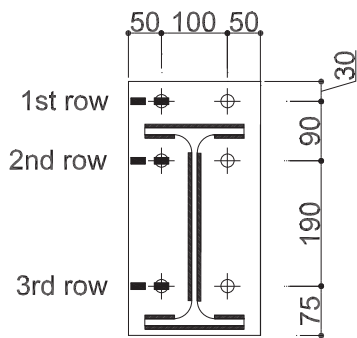
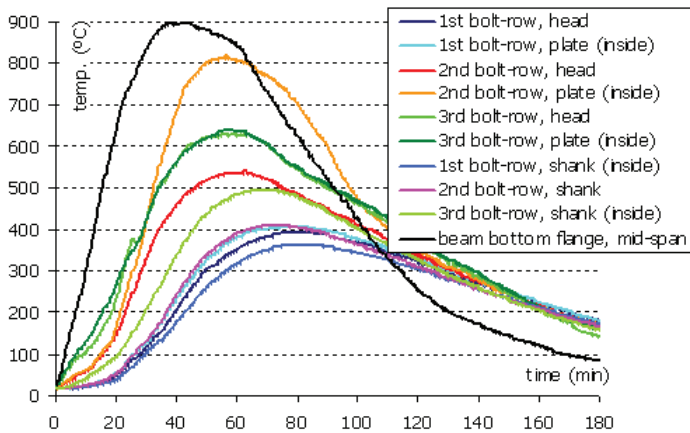


Fig. 12. Temperature within the joint Z3 (test EJ01).

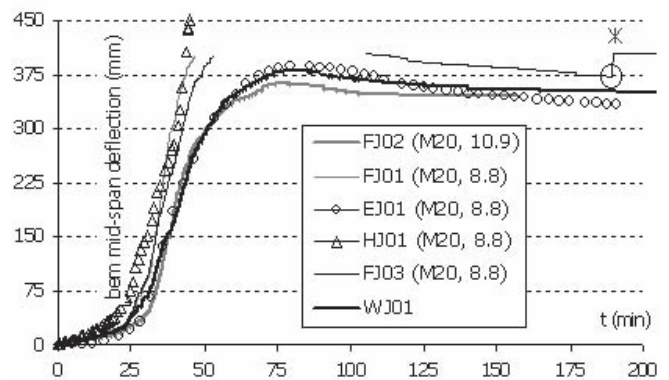


Fig. 13. Mid-span deflection of the beams.

(15.7 in.); moreover, it was possible to identify the failure of the bottom bolt row at  $t = 190$  min after the beginning of the fire; the top bolt row fractured later ( $t = 382$  min). Figure 14 shows the deformed structure at the end of the FJ01 test.

Based on the vertical displacement measured 300 mm (11.8 in.) away from the column end plate surface,  $d_{z3}$ , the joint rotation,  $\phi$ , is defined as:

$$\phi = \alpha + (\theta_b - \theta_c) = \tan^{-1} \left( \frac{d_{z3}}{300} \right) \quad (1)$$

where  $\alpha$  is the contribution from the shear deformation of the column web, and  $(\theta_b - \theta_c)$  the change in angle between the centerlines of the beam and column. In these tests, the column hardly deforms as it behaves as a rigid element. Then, both  $\alpha$  and  $\theta_c$  are neglected. Figure 15 shows the corresponding rotation curves.



Fig. 14. Deformed structure after test FJ01.

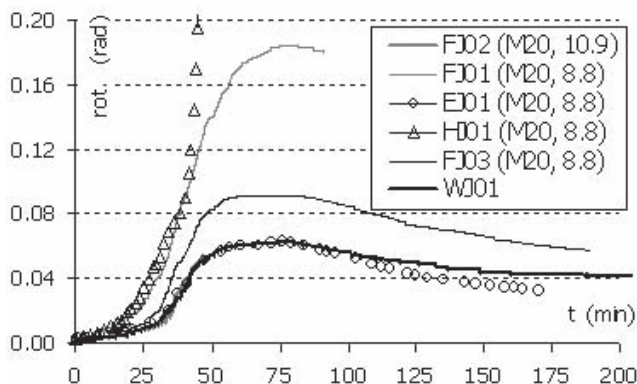


Fig. 15. Joint rotation.

## Failure Modes

The six subframe tests revealed distinct behaviors depending on the joint detail. In general terms, one configuration collapsed during the heating phase (HJ01) and three others during the cooling phase (FJ02, FJ03 and EJ01), although in the latter case it was possible to stop the test prior to complete collapse because of safety reasons. The main failure modes observed in the joints of the tested structures are described next.

### Test FJ01

Deformation of the end plate was observed, accompanied by local buckling of the beam bottom flange and shear buckling of the beam web (Figure 16). The deformation at the top of the end plate was mainly observed during the heating phase, while deformation at the bottom developed during the cooling phase, due to the tensile force in this zone. Bearing failure of the end plate around the bolts, particularly near the top flange, was also observed. Bolts did not suffer any damage. This failure mode was not surprising due to the reduced thickness of the end plate [10 mm (0.39 in.)].

### Test FJ02

Failure modes were apparently similar to those observed for test FJ01: end plate deformation accompanied by local buckling on the beam bottom flange and shear buckling of the beam web (Figure 17a). The end plate deformation was smaller than for test FJ01, because of a thicker end plate [16 mm (0.63 in.)]. However, a clear difference was noted, in the form of nut stripping of the bolts (Figure 17b). This indicated a clear change in failure modes, whereby the bolts became critical in tension during cooling, despite being class 10.9.



Fig. 16. Joint deformation at test FJ01.

### Test FJ03

During the heating phase, local buckling on the bottom flange and shear failure at the web were noticed. At the same time, and due to the large joint bending moment, end plate deformation at top developed and the weld on the top flange was broken (Figure 18b). During cooling and due to the large tensile forces that developed during this phase, minor cracks on the weld at the bottom flange (both joints) were observed together with bolt failure in joint Z2 (Figure 18a). The bolt failure mode was by nut stripping: after 190 min. from the beginning of fire, the bottom bolt row fails while the top bolt row broke later ( $t = 382$  min).

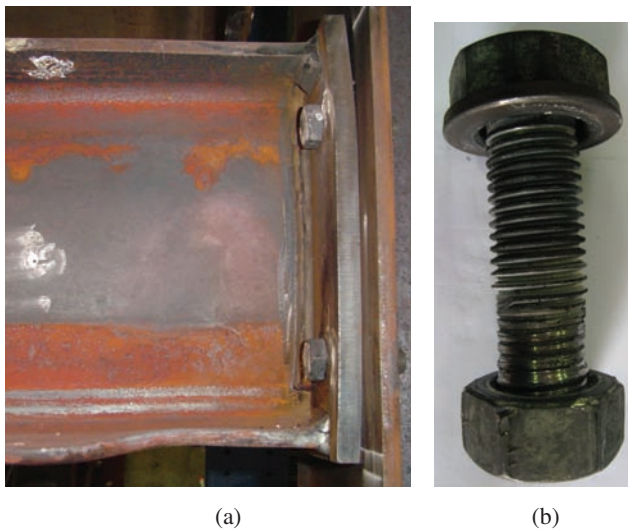


Fig. 17. (a) End plate deformation; (b) bolt stripping at FJ02.

### Test EJ01

During the heating phase, due to the end plate thickness of 16 mm (0.63 in.) and the connection configuration (three bolt rows), no significant end plate deformation developed; only deformation of the beam was observed: local buckling of the beam bottom flange and shear buckling of the beam web. However, during the cooling phase and due to the large tensile forces developed during this phase, localized deformation at the bottom of the end plate and failure (nut stripping) of the bottom bolt row was observed (Figure 19).

### Test HJ01

During the heating phase, local buckling on the bottom flange was observed; shear failure at the beam web was insignificant. At the maximum joint temperature of 850 °C (1,562 °F), the end plate broke along both beam web welds (joint Z3), because its tensile resistance is low and it had considerable rotation before the beam and column flange came into contact (Figure 20a). Rapidly, the beam suffered a large deflection, and shear forces were developed near the joint Z2, leading to beam rupture (Figure 20b). No damage to the bolts was observed. This failure mode was not observed in the other bolted joint, because they exhibit larger bending resistance.

### Test WJ01

During the heating phase, local buckling on the bottom flange was observed; shear failure at the beam web was minor (Figure 21). No damage to the welds was observed.

Furthermore, other failure modes were observed in the beam and in the concrete slab: shear buckling of the beam web near the load points; bursting of the concrete slab; large

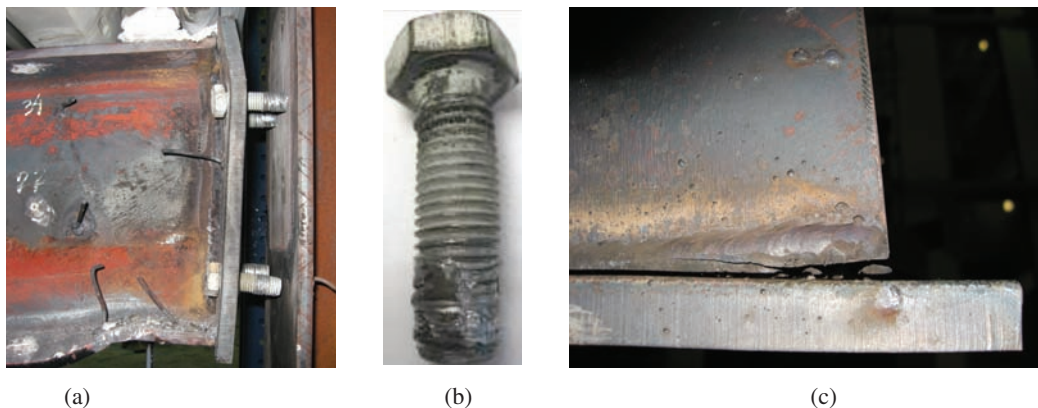


Fig. 18. (a) End plate deformation; (b) bolt stripping; (c) weld failure at test FJ03 (view from the top of the beam).

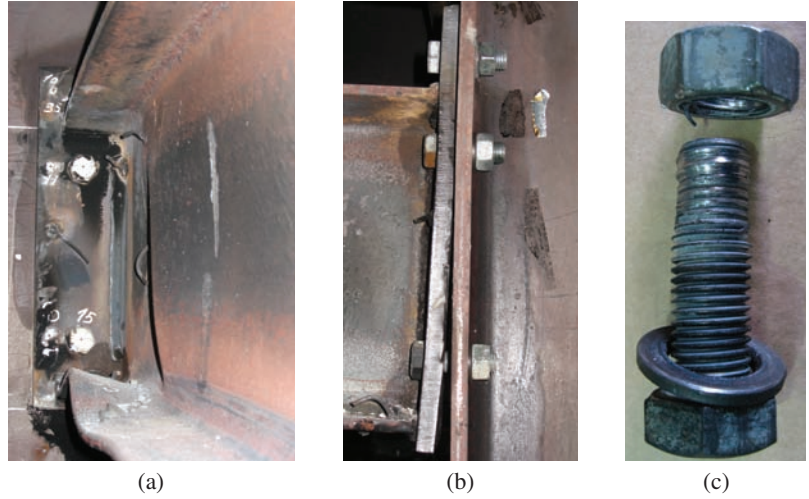


Fig. 19. (a) Local buckling on the beam bottom flange and web; (b) deformation at the bottom of the end plate; (c) nut and bolt stripping—bottom bolt row at test EJ01.

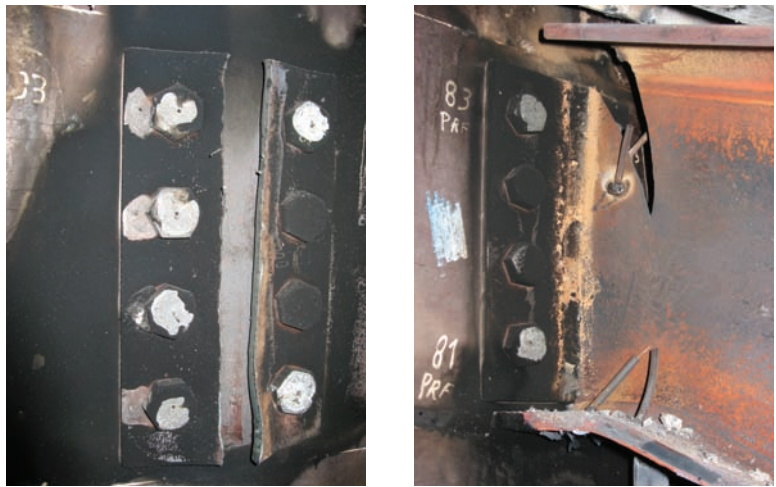


Fig. 20. (a) End plate failure (joint Z2); (b) beam failure (joint Z3) at test HJ01.



Fig. 21. Local buckling on the beam bottom flange and shear buckling of the beam web (joint Z2).

Table 7. Temperature Distribution Across the Depth of the Beam at Mid-span									
Test Location		Temperature (°C)							
		15 min.	25 min.	40 min.	50 min.	60 min.	70 min.	80 min.	150 min.
Average	bottom flange	477	729	893	897	857	748	646	170
	web	393	728	869	864	808	667	555	149
	top flange	273	563	772	809	793	704	595	204
Thermal gradients	bottom flange	$\theta_0$	$\theta_0$	$\theta_0$	$\theta_0$	$\theta_0$	$\theta_0$	$\theta_0$	$\theta_0$
	web	0.82 $\theta_0$	1.00 $\theta_0$	0.97 $\theta_0$	0.96 $\theta_0$	0.94 $\theta_0$	0.89 $\theta_0$	0.86 $\theta_0$	0.88 $\theta_0$
	top flange	0.57 $\theta_0$	0.77 $\theta_0$	0.86 $\theta_0$	0.90 $\theta_0$	0.93 $\theta_0$	0.94 $\theta_0$	0.92 $\theta_0$	1.21 $\theta_0$

$\theta_0$  = temperature of the bottom flange at beam mid-span

cracks on the concrete slab due to the separation of the shear studs from the concrete slab; major cracks perpendicular to the slab that occurred as a result of the beam and joints deformation (Figure 22). Due to the considerable size of the columns, column deformations are irrelevant.

### DISCUSSION

According to part 1-2 of Eurocode 3 (CEN, 2005c), the beam temperature is calculated as an average temperature within the cross-section that depends on the section factor and the temperature profile is assumed constant within the cross-section. These tests highlight the validity of this simplification adopted by the Eurocode, but only at elevated temperatures; at low temperature ( $t < 25$  min and  $t > 80$  min) the temperature profile is variable (Figure 23). Based on the

temperatures measured along the beam span, the temperature profiles as well as the thermal gradients, linked to different phases of the fire, could be calculated at the mid-span of the beam (Table 7). At low temperatures, the temperature profile is approximately linear and decreases from the bottom to the top flange. As the temperature increases, the temperature in the web increases at a faster rate and the profile becomes convex. At high temperatures, the top flange remains at a lower temperature, while the bottom flange and web show similar values. Finally, during the cooling phase, the temperature profile changes from convex to concave and the top flange now exhibits the highest temperature.

Similarly, based on the temperatures measured near the joints [200 mm (7.9 in.)], temperature profiles and thermal gradients linked to different stages of the fire are calculated where all temperatures are related to the bottom flange

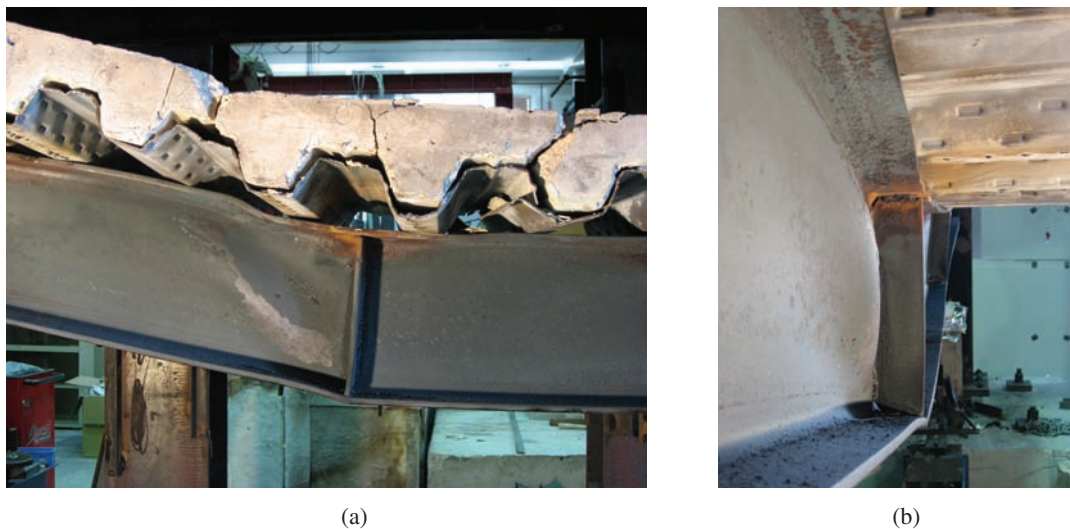


Fig. 22. Shear buckling of the beam web near the load points.

**Table 8. Temperature Distribution Across the Depth of the Beam Near the Joint**

Test Location		Temperature (°C)								EN 1993-1-2
		15 min.	25 min.	40 min.	50 min.	60 min.	70 min.	80 min.	150 min.	
Average	bottom flange	358	622	810	826	798	754	683	239	
	web	288	596	774	781	742	673	576	200	
	top flange	201	482	715	738	715	670	591	249	
Thermal gradients	bottom flange	0.75 $\theta_0$	0.85 $\theta_0$	0.91 $\theta_0$	0.92 $\theta_0$	0.93 $\theta_0$	1.01 $\theta_0$	1.06 $\theta_0$	1.41 $\theta_0$	0.88 $\theta_0$
	web	0.60 $\theta_0$	0.82 $\theta_0$	0.87 $\theta_0$	0.87 $\theta_0$	0.87 $\theta_0$	0.90 $\theta_0$	0.89 $\theta_0$	1.18 $\theta_0$	0.75 $\theta_0$
	top flange	0.43 $\theta_0$	0.66 $\theta_0$	0.79 $\theta_0$	0.82 $\theta_0$	0.83 $\theta_0$	0.89 $\theta_0$	0.92 $\theta_0$	1.49 $\theta_0$	0.62 $\theta_0$

$\theta_0$  = temperature of the bottom flange at beam mid-span.

temperature at mid-span, for the same time (Table 8). The experimental results show that the thermal gradient is not constant during a fire, changing from convex to concave with time. Figure 24 illustrates the proposed temperature gradients of EN 1993-1-2 (CEN, 2005c) that only depend on the beam height. It can be seen that the proposed Eurocode thermal gradients approximate the experimental results in the range 20 min < t < 40 min, which corresponds to a bottom flange temperature of circa  $\theta_0 = 830$  °C (1,526 °F).

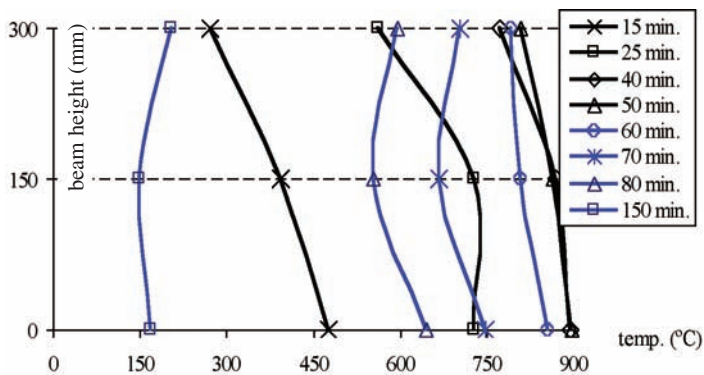


Fig. 23. Temperature profiles across the depth of the beam near the joint.

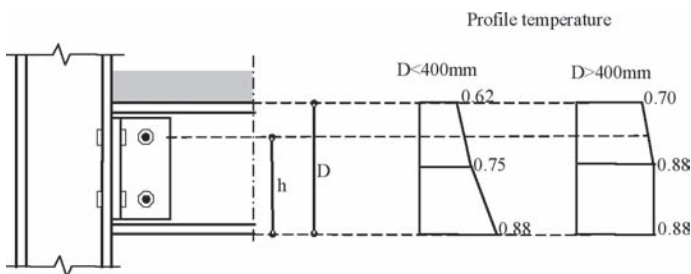


Fig. 24. Thermal gradient across the depth of a composite joint (CEN, 2005c).

Based on the measured axial and vertical displacements of the beam and the axial stiffness of the beam and end restraints, it is possible to estimate the axial force in the beam and the bending moment at the joints. Figures 25 and 26 illustrate the variation of the axial force and bending moment with time.

It can be seen that the joints are subjected to a varying axial force and bending moment throughout the fire event, from an initial state of pure bending. This complex stress state, combined with the M-N resistance interaction diagram for a given temperature profile in the joint, explains the observed behavior of each joint.

HJ01 was the only connection that failed during the heating phase. The header plate failed at the maximum temperature because of lack of resistance to the developed bending moment arising from very large rotations.

Joints EJ01, FJ03 and FJ02 failed during the cooling phase, in a mode 3 failure of the bottom bolt row (CEN, 2005b). These three joints share the same thickness of the

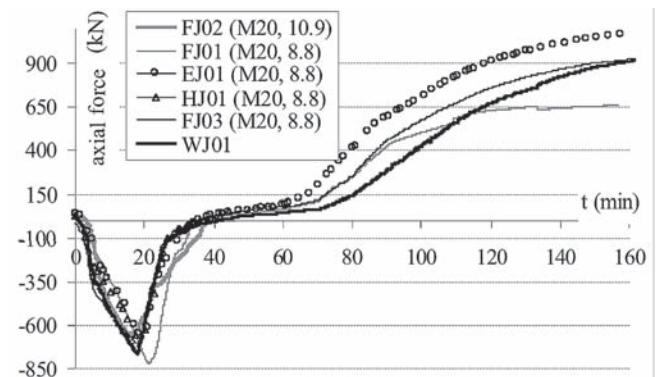


Fig. 25. Axial forces using the average temperature at the beam mid-span.

Table 9. Axial Force and the Tensile Resistance of the Bolts at Failure			
	No. of Bolts	$N_{Ed}$	$F_{ten,t,Rd}$
EJ01	6	1,065 kN (239 lbf)	1,330 kN (239 lbf)
FJ03	4	900 kN (202 lbf)	688 kN (154 lbf)
FJ02	4	–	890 (200 lbf)

end plate [16 mm (0.63 in.)], which prevented plastic stress redistributions within the joint and, consequently, a reduction of the applied bolt row force at the level of the bottom bolt row. As a rough approximation, based only on the axial force, Table 9 compares the applied axial force and the tensile resistance of the bolts at failure.

In Table 9, the tensile resistance of each bolt is given by

$$F_{ten,t,Rd} = \frac{0.9k_{b,\theta}f_{ub}A_s}{\gamma_{Mfi}} \quad (2)$$

where  $A_s$  is the tensile stress area of the bolt,  $\gamma_{Mfi}$  is the partial safety factor for the relevant material property, for the fire situation (taken as 1.0),  $f_{ub}$  is the ultimate stress of the bolts, and  $k_{b,\theta}$  is the reduction factor determined for the appropriate bolt temperature, taken as  $k_{b,\theta} = 0.935$  [evaluated for a temperature of about  $\theta_b = 200$  °C (392 °F), corresponding to the bolt temperature at failure]. For joint EJ01, it is clear that failure of the bolts is inevitable because of the presence of a bending moment that causes the tensile force to flow through the bottom bolts. It is noted that considering only the four bolts in tension,  $F_{ten,t,Rd}$  reduce to 688 kN (155 lbf). Joints FJ03 and FJ02 also exhibit tensile failure of the bolts, more pronounced for FJ03 because of the lower grade of the bolts.

Joint FJ01, in contrast, survived the fire event in spite of a lower moment resistance because of the extra ductility provided by a thinner plate of 10 mm (0.39 in.). Joint WJ01 also survived the fire event.

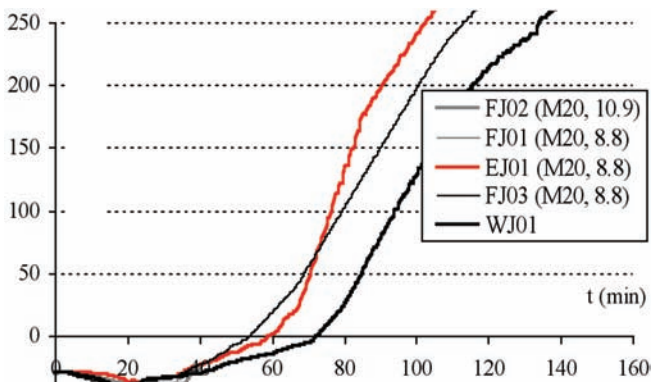


Fig. 26. Internal bending moment at the joints.

## CONCLUSIONS

This paper reports on an experimental investigation on the fire behavior of a steel substructure consisting of an unprotected steel beam and connections and two fire-protected columns. Six subframes were tested whereby only the beam-to-column joints were varied. In line with current design trends, PR semi-rigid joints (at ambient temperature) were chosen, ranging from a welded configuration to several end plate typologies. In addition, for the fire loading, a relatively low applied live load ratio of 0.2 was applied (because of testing limitations).

The experimental results for the six tests show a clear influence of the joint typologies on the overall response of the subframe. The tests demonstrated the appearance of large tensile forces and the reversal of bending moment during the cooling phase, already shown numerically by the authors (Santiago et al., 2008). They also demonstrated that these forces may result in failure of the joint, as was already postulated by the authors in previous works (Simões da Silva et al., 2005).

Finally, these test results give clear indication on how to propose design guidance to avoid failure of the joints under fire loading, in the framework of the component method under fire conditions (Simões da Silva, Santiago, Vila Real and Moore, 2002). The proposed concept, for joints where the column web panel is fire protected (as was the case for these tests), is to make sure that failure of the tensile components (T-stub in tension) is controlled by the ductile end plate (mode 1) and not the bolts, both for hogging and sagging moments. This is a direct consequence of the reversal of bending moment and the subsequent M-N interaction during the cooling phase. In practical terms, this means that for most situations stronger or larger bolts should be applied in the bottom bolt row of the connection. Further details on design issues can be found in Santiago et al., 2008.

## ACKNOWLEDGMENTS

Financial support from the Portuguese Ministry of Science and Higher Education (Ministério da Ciência e Ensino Superior) under contract grant POCI/ECM/55783/2004 is gratefully acknowledged.

## REFERENCES

- Al-Jabri, K.S. (1999), "The Behavior of Steel and Composite Beam-to-Column Connections in Fire," Doctoral Thesis, University of Sheffield, UK.
- Allam, A.M., Fahad, M.K., Liu, T.C.H., Burgess, I.W., Plank, R.J. and Davies, J.M. (1999), "Effects of Restraint on the Behavior of Steel Frames in Fire," *Proc. Conference Eurosteel '99*, Praha, Czech Republic.
- Bailey, C.G., Lennon, T. and Moore, D. (1999), "The Behavior of Full-Scale Steel-Framed Building Subjected to Compartment Fires," *The Structural Engineer*, Vol. 77, No. 8, pp. 15–21.
- Buchanan, A.H. (2002), *Structural Design for Fire Safety*, John Wiley & Sons, England.
- CEN (1992), *Eurocode 3: Design of Steel Structures—NP EN 10002-5: 1992*, European Committee for Standardization, Brussels, Belgium.
- CEN (1995), *Eurocode 3: Design of Steel Structures—ENV 1993-1-2: 1995*, European Committee for Standardization, Brussels, Belgium.
- CEN (2004), *Eurocode 3: Design of Steel Structures—NP EN 10025-1: 2004*, European Committee for Standardization, Brussels, Belgium.
- CEN (2005a), *Eurocode 3: Design of Steel Structures—EN 1993-1-1: 2005*, European Committee for Standardization, Brussels, Belgium.
- CEN (2005b), *Eurocode 3: Design of Steel Structures—EN 1993-1-8: 2005*, European Committee for Standardization, Brussels, Belgium.
- CEN (2005c), *Eurocode 3: Design of Steel Structures—EN 1993-1-2: 2005*, European Committee for Standardization, Brussels, Belgium.
- Lawson, R.M. (1990), "Behavior of Steel-Beam-to-Column Connections in Fire," *The Structural Engineer*, Vol. 68, No. 14, pp. 263–271.
- Leston-Jones, L.C. (1997), "The Influence of Semi-Rigid Connections on the Performance of Steel Framed Structures in Fire," Doctoral Thesis, University of Sheffield, UK.
- Liu, T.C.H., Fahad, M.K. and Davies, J.M. (2002), "Experimental Investigation of Behavior of Axial Restrained Steel Beams in Fire," *Journal of Constructional Steel Research*, Vol. 58, pp. 1211–1230.
- Santiago, A. (2008), "Behavior of Beam-to-Column Steel Joints Under Natural Fire," Doctoral Thesis, Department of Civil Engineering, University of Coimbra, Coimbra, Portugal.
- Santiago, A., Simões da Silva, L. and Vila Real, P. (2008), "Fire Design of Bolted Steel Beam-to-Column Joints," *Proce. International Workshop on Connections in Steel Structures: Connections VI*, Chicago, IL.
- Simões da Silva, L.A.P., Santiago, A. and Vila Real, P. (2002), "A Component Model for the Behavior of Steel Joint at Elevated Temperatures," *Journal Constructional Steel Research*, Vol. 57, No. 11, pp. 1169–1195.
- Simões da Silva, L., Santiago, A., Vila Real, P. and Moore, D. (2005), "Behavior of Steel Joints Under Fire Loading," *Steel and Composite Structures*, Vol. 6, pp. 485–513.
- Wald, F., Simões da Silva, L., Moore, D., Lennon, T., Chladna, M., Santiago, A., Benes, M. and Borges, L. (2006a), "Experimental Behavior of a Steel Structure Under Natural Fire," *Fire Safety Journal*, Vol. 41, No. 7, pp. 509–522.
- Wald, F., Chladná, M., Moore, D., Santiago, A. and Lennon, T. (2006b), "Temperature Distribution in a Full-Scale Steel Framed Building Subject to a Natural Fire," *International Journal of Steel and Composite Structures*, Vol. 6, No. 2, pp. 159–182.